NASA MEMO 3-16-59W

NASA

MEMORANDUM

EFFECT OF CASCADE PARAMETERS ON ROTATING STALL

By A. H. Stenning, B. S. Seidel and Y. Senoo
Massachusetts Institute of Technology

NATIONAL AERONAUTICS AND SPACE ADMINISTRATION
WASHINGTON
April 1959

NATIONAL AERONAUTICS AND SPACE ADMINISTRATION

MEMORANDUM 3-16-59W

EFFECT OF CASCADE PARAMETERS ON ROTATING STALL

By A. H. Stenning, B. S. Seidel
and Y. Senoo

SUMMARY

Analysis of the vortex model proposed by Kriebel, Seidel, and Schwind shows this representation of rotating stall satisfies, at least approximately, the requirements at the cascade. Cascade-parameter-variation effects on rotating stall were studied in a circular cascade and single-stage compressor. Modification of the single-stage compressor stopped the rotating-stall pattern and permitted observation of the pressure and velocity distribution around the annulus. Closer observation might be possible with proper flow-visualization techniques, such as a water pump.

INTRODUCTION

The present report covers part of an investigation of stall propagation in cascades and compressors which has been carried out at the Gas Turbine Laboratory of Massachusetts Institute of Technology under the sponsorship and with the financial support of the National Advisory Committee for Aeronautics. This study investigates in detail the mechanism of stall propagation in order to obtain improved methods of control through a better understanding of the phenomenon.

In the first part of the investigation a small perturbation analysis of rotating stall in a cascade was developed and compared with the available test data and with information obtained from the Gas Turbine Laboratory circular cascade and single-stage compressor (refs. 1 and 2). This analysis considered the stability of the flow under the two limiting conditions which represented the best estimate of the bounds on the behavior of the fluid downstream of the cascade. Conditions for the initiation of rotating stall and expressions for propagation velocity were obtained. The stability criterion, which was the same as that derived earlier by Emmons (ref. 3), states that rotating stall becomes possible when $\frac{dC_p}{d\beta_1}$ is equal to $-2 \cot \beta_1 (1 - C_p)$ if β_2 is constant.

Comparison of the stability criterion with a number of cascade and stage tests (refs. 1 to 4) indicates that rotating stall occurs with $dC_p/d\beta_1$ equal to or greater than the predicted numerical value. Observed propagation velocities fell between the values predicted for the two extreme cases and showed no consistent agreement with either. Since the fully developed stall propagation phenomenon is highly nonlinear, close agreement with any linearized small perturbation and analysis is unlikely.

During the early phase of the experimental investigation the number of stall cells in the circular cascade was considerably larger than the number usually observed in compressors, and the frequency of stalling of one airfoil approached the Kármán vortex frequency as the solidity of the cascade was reduced. In addition, small regions of very low density were observed in some schlieren photographs after an airfoil stalled. These observations suggested the presence of vortices in the unsteady flow, and later in the investigation high-speed interferograms were taken of the flow in the cascade, showing clearly that when one of the airfoils stalled, all of the shed circulation departed in the form of a single vortex followed by a starting vortex when the airfoil unstalled. A new theoretical model of rotating stall was constructed and was found to agree well with observations in the single-stage compressor as well as in the cascade (ref. 5).

Unfortunately, neither of the analyses gave a clear answer to the problem of determining the number of stall cells to be expected in a given configuration, and the unsteadiness of the phenomenon made observation of the cell-splitting process exceedingly difficult. The small perturbation analysis indicated that the time-dependent boundary-layer response might be a governing factor. The vortex model suggested the additional hypothesis that stall-cell splitting might be produced when the width of the stall-cell exceeded a critical value depending on the length of the cell downstream, although it appears that this predicted value is too large to be of practical importance in most cases.

The major effort during the final phase of the study has been directed toward the following objectives:

(1) The behavior of the vortex model close to the cascade has been studied to answer some questions that arose during the original analysis.

(2) The effect of variation of cascade parameters on rotating stall was investigated by changing the wall configuration, camber, and stagger in the circular cascade and by changing the airfoil shape in the compressor.

(3) The extreme difficulty of obtaining any useful data on the process of stall-cell splitting when the cell is rotating suggested the desirability of designing a compressor stage with sufficient counterrotation ahead of the rotor to stop the stall cell relative to the casing and

thus facilitate observation. This result was accomplished by modification of the single-stage compressor, and several runs were made with the stall cell stationary or rotating in the direction opposite to the rotor.

The contribution made by Mr. K. Isaksen during a thesis investigation is gratefully acknowledged.

SYMBOLS

b	width of stall cell
C	absolute fluid velocity
C_p	cascade pressure coefficient
C_r	radial velocity
F	pressure recovery factor
L	blade chord
p	static pressure
p_o	stagnation pressure
p'	mean static pressure
r	distance from vortex
s	blade spacing
t	time
Δt	time increment
U	blade speed
u	induced x-velocity
V	fluid velocity relative to stall cell
V_p	propagation speed of stall cell relative to cascade
v	induced y-velocity
W	fluid velocity relative to cascade
X	coordinate along cascade axis
Y	coordinate normal to cascade axis

α absolute fluid angle

β fluid angle relative to cascade

Γ vortex strength or circulation

Γ_o circulation outside blade cell

Γ_s shed vorticity

γ mean fluid angle relative to stall cell

ρ fluid density

λ blade stagger angle

σ cascade solidity, ratio of chord to spacing

Subscripts:

m mean condition

x axial component of velocity

θ tangential component of velocity

1 upstream of cascade (inlet in circular cascade)

2 downstream of cascade

FURTHER CONSIDERATIONS OF VORTEX ANALYSIS

In reference 5, with the assumptions that an airfoil loses all its circulation when it enters a stall cell and that the axial velocity within the stall cell is zero, the requirements of conservation of vorticity and mass were employed to derive the following expression for the propagation velocity of the stall cell:

$$\frac{V_p}{W_{\theta,1}} = 1 \pm \sqrt{1 - \left(\frac{W_2}{W_{\theta,1}}\right)^2} \qquad (1)$$

where W_2 is the velocity outside the stall cell downstream of the blade row and $W_{\theta,1}$ is the tangential velocity far upstream. The assumption that the circulation drops to zero in the cell is a reasonable one if the

velocity in the cell is zero since the airfoil can have no lift when it is surrounded by stationary fluid. However, no theoretical justification could be found for the assumption of zero velocity although measured velocities within the cell were very close to zero. The analysis did not consider the conditions in the region close to the cascade, and it was thought that an analysis of the flow at the cascade would yield additional requirements which would permit a complete solution without assuming a value of the velocity within the stall cell. The difficulty of obtaining a closed solution for the motion of an infinite number of vortices led to the adoption of a numerical approach, which is described later. However, a simple analysis of the equilibrium of the stall cell at the cascade has clarified some of the questions raised by the original analysis.

EQUILIBRIUM OF STALL CELL AT CASCADE

If the stall cell, shown in figure 1, is considered as a region that has an axial velocity of zero, moving along the cascade with velocity V_p and removing the circulation from the unstalled airfoils as it passes over them, then the Kriebel, Seidel, and Schwind analysis (ref. 5) yields equation (1) for the propagation velocity. If the flow outside the stall cell is loss-free, equation (1) reduces to

$$\frac{V_p}{W_{\theta,1}} = 1 \pm \sqrt{1 - \frac{(1 - C_p)}{\sin^2\beta_1}} \tag{2}$$

This analysis does not consider the equilibrium of the front face of the stall cell, and it remains to be seen whether this region is in balance. The flow is steady with respect to an observer on the stall cell if the vorticity is spread out over a line instead of being concentrated in vortices. The control volume around the front face of the stall cell shown in figure 1 indicates that there is no momentum flux through the control volume and no lift on the airfoils so that the integrated pressure forces on the control volume must be zero for equilibrium. The flow around the front of the stall cell is essentially the same as that around a flat plate inclined at a large angle to the flow, and the mean pressure on the front must therefore be almost equal to the stagnation pressure relative to the stall cell (ref. 6). If p' is the mean static pressure on the front of the stall cell, $p' = p_1 + F \frac{\rho}{2} V_1^2$ where V_1 is the velocity of the fluid upstream relative to the cell, and F is of the order of 0.8 to 0.9, depending on the angle made by the vector V_1 with the face of the cell. If the pressure downstream of the cascade is constant and equal to p_2, then

$$p' = p_2 = p_1 + F \frac{\rho}{2} V_1^2 \tag{3}$$

for equilibrium.

Now

$$V_1^2 = W_{x,1}^2 + (W_{\theta,1} - V_p)^2$$

$$= W_1^2 + V_p^2 - 2W_{\theta,1}V_p$$

Therefore

$$p_2 = p_1 + F\frac{\rho}{2}\left(W_1^2 + V_p^2 - 2W_{\theta,1}V_p\right)$$

But

$$p_2 - p_1 = C_p\frac{\rho}{2}W_1^2$$

Then

$$C_p\frac{\rho}{2}W_1^2 = F\frac{\rho}{2}\left(W_1^2 + V_p^2 - 2W_{\theta,1}V_p\right)$$

Solving for V_p results in the following equation:

$$\frac{V_p}{W_{\theta,1}} = 1 \pm \sqrt{1 - \frac{(F - C_p)}{F\sin^2\beta_1}} \qquad (4)$$

Earlier considerations of the vortex motion led to the rejection of the larger value because it was incompatible with the actual propagation mechanism. Equation (4) is interesting because it has almost the same form as equation (2), and, if $F = 1$, the two expressions are identical. Put in physical terms, the stall cell must move with a velocity sufficient to reduce the stagnation pressure relative to the stall cell to a value that can be balanced by the pressure downstream. To satisfy this requirement, the cell moves in the direction of $C_{\theta,1}$. Stall cells of this type can exist only for diffusing cascades with C_p greater than the critical value $(F - \sin^2\beta_1)$.

From the preceding simple analysis of the equilibrium of the front of the stall cell, it can be seen that the Kriebel, Seidel, and Schwind assumption of zero velocity within the stall cell satisfies, at least approximately, the requirements at the cascade.

NUMERICAL ANALYSIS OF VORTEX TRAJECTORIES

In order to obtain detailed information about the flow close to the cascade, a numerical calculation of the vortex motion was carried out using a Burroughs digital computer. The problem was approached by considering the flow field from the point of view of an observer on the stall cell. In this reference frame, airfoils approach the stall cell with velocity V_p, release their circulation as they enter the cell, and regain it when they leave (fig. 2). A starting vortex is shed by each airfoil when it unstalls. If an arbitrary propagation velocity and cell width are chosen and the airfoils are fed into the stall cell with this velocity, the vortex trajectories may be found, and the periodic variation in angle of attack at the ends of the cell computed. If the values of V_p and b chosen are the correct ones for the cascade, the angle of attack at the upper end of the cell will attain the stalling value at the instant when an airfoil enters the cell and sheds its circulation, and the angle of attack at the lower end of the cell will return to the unstalling value just at the instant when the airfoil regains its circulation. If the values of V_p and b chosen are not the correct ones, the angles of attack will not match the cascade characteristic, which might be of the form shown in figure 3, and the calculation must be repeated with new values. A high-speed computer could be programmed to hunt for the correct solution, but the present study was limited to a study of the feasibility of the basic calculation and the completion of a trial case. The problem is defined by selecting values of s/b, $\Gamma_o/V_m s$, Γ_s/Γ_o, γ, V_p/V_m, s/L, and λ. Auxiliary information to determine the location along the chord of the bound vortex and the initial point of the shed vortices is also required. An upper bound to the number of vortices in the field is set by the memory capacity of the computer.

A shed vortex moves with a velocity determined by summing the velocities induced upon it by all the other vortices and adding the effect of the streaming flow V_m. Thus, if the motion of the K^{th} vortex is to be found,

$$\frac{u_K}{V_m} = \sum_{n \neq K} \left[\frac{\frac{\Gamma_n}{V_m s}\left(\frac{Y_K}{s} - \frac{Y_n}{s}\right)}{2\pi\left(\frac{r_n}{s}\right)^2} \right] + \frac{V_m \cos \gamma}{V_m} \tag{5}$$

$$\frac{v_K}{V_m} = -\sum_{n \neq K} \left[\frac{\frac{\Gamma_n}{V_m s}\left(\frac{X_K}{s} - \frac{X_n}{s}\right)}{2\pi\left(\frac{r_n}{s}\right)^2} \right] + \frac{V_m \sin \gamma}{V_m} \tag{6}$$

$$\left(\frac{X_K}{s}\right)_{t+\Delta t} = \left(\frac{X_K}{s}\right)_t + \frac{u_K}{V_m}\left(\frac{V_m}{s}\Delta t\right) \tag{7}$$

$$\left(\frac{Y_K}{s}\right)_{t+\Delta t} = \left(\frac{Y_K}{s}\right)_t + \frac{v_K}{V_m}\left(\frac{V_m}{s}\Delta t\right) \tag{8}$$

Similarly, the local incidence on the airfoils entering and leaving the stall cell may be calculated by finding the induced velocities ahead of the airfoils.

A single (one choice of V_p/V_m) computation of the type described was carried out on a Burroughs E 101 electronic computer. Representative values of the parameters were chosen and are as follows:

$$s/b = 1/7;\ \Gamma_o/V_m s = 0.616;\ V_p/V_m = 0.595$$

$$\gamma = 36^\circ;\ \lambda = 30^\circ;\ s/L = 1.0;\ \Gamma_s/\Gamma = 1.0$$

The location of the bound vortex along the chord and the initial point for the shedding of the vortices are shown in figure 2. The choice of the latter point was governed by the considerations given by Kriebel, Seidel, and Schwind in reference 5. The calculation was commenced with 20 airfoils on each side of the cell, the number being limited by the capacity of the computer. Figures 4 and 5 present the results of this calculation. In figure 4, the circles mark the positions of the shed vortices at a given time after several airfoils have passed through the stall cell. The lines show the trajectory of each vortex. The rapid convergence of the calculation is indicated by the close correspondence of the trajectories of the last three vortices shed at each end of the stall cell.

The possibility of the stall-cell configuration being governed by the stability requirements of the vortex street had been suggested during the experimental investigation and, although there was no experimental evidence that the street arranged itself in a definite pattern, still the hypothesis had not been definitely disproved. However, the computed vortex trajectories showed no instability development, and the street seemed to be growing in an orderly manner with the expected tendency to roll up at the ends. The result suggests that the vortex street does not influence the size of the stall cell since the vortices apparently accommodated themselves to the completely arbitrary dimensions of the cell.

Figure 5 shows the values of inlet angle at the ends of the stall cell relative to the cascade. The calculation converges rapidly, and

after four cycles the process is essentially periodic. Vortices are released from the ends of the cell at 0, 1, 2, 3, and so forth. At the upper end of the cell, the inlet angle attains a maximum value of 76° just before the vortex is released; this may be regarded as the angle at which stall occurs. At the lower end of the cell the inlet angle is 54° when the airfoil unstalls; therefore, for the assumed stall-cell configuration a cascade characteristic with hysteresis would be required. In addition, it would be desirable to follow the angle at the leading edge of one airfoil as it passes through the cell to ensure that the value of 54° is not attained before reaching the bottom of the cell. If the true cascade characteristic were one with no hysteresis, V_p or b or both would have to be adjusted until $\beta_{\text{Upper end}} = \beta_{\text{Lower end}}$ at stall and unstall.

The calculation method appears satisfactory and could be refined to include cascade characteristics more complex than that shown in figure 3.

EFFECT OF CASCADE PARAMETERS ON ROTATING STALL

During the course of the experimental program, repeated attempts have been made to secure some control over the number of stall cells in the circular cascade and single-stage compressor by systematic variation of cascade parameters. As reported previously (refs. 1 and 5), the number of stall cells found in the circular cascade has always been between nine and twenty, with the exception of one case in which five cells were apparently present. Increasing the radial spacing between the nozzle row and the diffusing blade row from 1 chord length to 2 had no effect on the number of cells although it is possible that a more substantial increase in spacing would have caused some change in the pattern. When the solidity of the diffusing cascade was changed in steps from 1 to 1/3, no significant change in the number of cells was observed. Changing the stagger of the cascade did not affect the number of cells, neither did removal of the wall boundary layer upstream of the cascade. Experiments on rectilinear cascades carried out at Harvard University (ref. 3) and Cambridge University (ref. 7) have yielded similar results with stall-cell wavelengths of the order of only three or four blade spacings instead of the ten to thirty customarily found in compressors.

The single-stage compressor, on the other hand, did not usually have more than four stall cells. Of all the blade-row configurations tested, only one (a set of guide vanes followed by a rotor) had more than four cells. In this case, eight or nine cells were observed when rotating stall commenced. These cells broke down into the familiar one, two, three, four sequence as the flow was reduced.

The substantial step in size from the small cells to the large ones suggests the possibility of two governing mechanisms that control the

small cell and large cell regimes, respectively. The inability to determine the governing parameters makes an analytical approach exceedingly difficult since there are few suggestions as to the best approach. In consequence, a continued program of testing different cascade configurations has been maintained, in spite of the unsatisfactory results of such work in the past, because the only possibility of solving the problem at present appears to be in a continuation of experimental work until some pattern emerges. The results of the final phase of this program are described in the next section.

VARIATION OF DOWNSTREAM WALLS IN CIRCULAR CASCADE

In the original circular cascade, the bounding side walls of the cascade continued only a few chord lengths downstream of the diffusing blades with a sudden expansion into a scroll of large cross section (fig. 6). This sudden expansion so close to the cascade presumably imposed a substantially constant pressure around the circumference on the outlet side of the cascade. In addition, the vortex street bounding a stall cell was presumably destroyed when it entered the scroll because air would be drawn into the vortex cores from the open sides. If the Kriebel, Seidel, and Schwind hypothesis about the factors governing the stall-cell size (ref. 5) were correct, it would be possible to increase the width of the cells by extending the walls downstream of the cascade and thus increasing the length of the stall cells. Accordingly, the side walls were extended 4 inches all around the test section and earlier tests repeated, using configuration B of reference 5, with the circular cascade set at a stagger of 31° and a solidity of 1.0.

The walls had no detectable effect on cascade performance, number of cells, or velocity of propagation. It is concluded that the sudden expansion after the cascade is not responsible for the large number of cells.

HIGH-CAMBER BLADES IN CIRCULAR CASCADE

All previous work in the circular cascade had been carried out with the same set of blades, modified 65-series airfoils of low camber. To study the effect of camber upon rotating stall, a set of 65(18)10 airfoils was made and tested in the circular cascade with stagger angles of 31° and 0°, measured from the radial direction. The blade chord was 1.00 inch, and the cascade solidity 1.00 at the leading edge. The low Mach number performance of the cascade at 31° stagger angle is shown in figure 7 with and without extended side walls. The pressure-rise characteristic of the cascade was altered slightly by the side walls, but rotating stall occurred at the same angles in both cases and was of the same type. After a first peak in the C_p curve at a β_1 of 53°, the pressure coefficient

fell and rose again to a second peak at a β_1 of 61°. In the vicinity of the second peak some random stall occurred, but periodic rotating stall did not commence until β_1 reached 65°, at which point eight to ten cells were observed and propagated with a $V_p/C_{\theta,1}$ of 0.32. As in all the previous studies, not more than two adjacent blade passages were stalled at any time (fig. 8). This pattern of stall cells persisted up to an inlet angle of 71°, at which point a combination of stall propagation and surge phenomenon was observed, with some reverse flow occurring in blade passages before the propagating stall reached them (fig. 8(b)). The stall cell was still visible, but appeared to be accompanied by an over-all surging process, which confused the schlieren photographs and prevented an accurate analysis of the number of cells and their velocity of propagation. As β_1 was increased beyond 71°, the surging became more pronounced until at 83° no sign of stall propagation could be seen, and the flow in the portion of the cascade visible in the window consisted only of a confused motion of highly turbulent air with frequent flow reversals in the individual passages (fig. 8(c)). The schlieren pictures with and without extended side walls show that the side walls had no visible effect on the phenomenon.

The stagger of the cascade was next changed to zero. The purpose of this change was to investigate the possibility of rotating stall occurring with a pressure drop, instead of a pressure rise, across the cascade. The small perturbation theory shows no preference in this respect, requiring only that $dC_p/d\beta_1$ attain a critical negative value for rotating stall to be possible. The large perturbation analysis with zero velocity within the cell requires a definite positive value of C_p to permit a pressure balance across the stalled portion of the cascade. The performance of the cascade at zero stagger is shown in figure 9. There was at all times a pressure drop across the cascade, although it had a minimum value at an inlet angle of 42°. In spite of the fact that C_p was always negative, the C_p against β_1 curve had the usual shape. Rotating stall was first found at an inlet angle of 44° (fig. 10) with a $dC_p/d\beta_1$ of -6. The theoretical value of $dC_p/d\beta_1$ from the linearized theory for rotating stall to be possible was -2.5. The cells propagated very slowly with $V_p/C_{r,1}$ only 0.34. However, $V_p/C_{\theta,1}$ was 0.35, so that the change in propagation velocity appeared to be caused by the reduction in inlet tangential velocity. There were eleven cells present, and the predicted value of $V_p/C_{\theta,1}$ from the simple linearized theory with no pressure variation behind the cascade was 1.0 (in error by a factor of 3). The vortex-shedding analysis with zero velocity in the stall cell would give no solution for propagation velocity in this case.

The schlieren photographs show that the passages were never completely stalled; some flow always passed through them. This case is therefore closer to the small rather than to the large perturbation model. For inlet angles higher than 49° the rotating stall disappeared and the cascade was fully stalled.

Figure 11 shows a summary plot of experimental values of $V_p/C_{\theta,1}$ for the circular cascade at a solidity of 1.0. It is remarkable that no consistent effect of camber, stagger, or inlet angle on propagation velocity can be seen. Most of the experimental points lie between $V_p/C_{\theta,1}$ of 0.30 and 0.34.

EFFECT OF AIRFOIL PROFILE ON ROTATING STALL IN ISOLATED ROTOR

In the experimental program on the circular cascade, every major variable but profile shape was investigated. It was therefore suggested that the blading used in the experiments on an isolated rotor in the single-stage-compressor stand (ref. 5) should be replaced by blading with a different profile shape but the same design-point performance.

The original blades had NACA 0010 thickness distribution on a circular-arc camber line with a 30.3° camber. The section was the same at all radii with a 9.7° twist from root to tip. The stagger at the mean radius was 52.7° and the solidity was 1.02. These blades were replaced by NACA 65(12)10 profiles, having the same twist, solidity, and stagger, and the same design-point deflection. The hub-tip ratio of the compressor was 0.75 and the tip radius was 11.63 inches.

With the usual instrumentation for total and static pressures and with hot wires to determine the number and frequency of the stall cells, the low Mach number performance of the isolated rotor was investigated at the mean radius. The air entered the rotor axially, there being no inlet guide vanes. The rotor performance in terms of C_p against the mean radius value of β_1 is presented in figure 12 with the performance of the original blading superimposed for comparison. The performance of the two blade rows was very similar in and out of stall. In both blade rows rotating stall commenced with one stall cell. As flow was decreased the stall pattern changed to two cells and then to an unsteady region of three or four cells. The stall propagation velocity in the 65-series blading was slightly lower than in the circular-arc blading (fig. 13) in agreement with the trend predicted by equation (2), since the 65-series blading had the higher pressure coefficient. As in previous configurations, $V_p/C_{\theta,1}$ was practically constant over the rotating-stall range.

INVESTIGATION OF A CASCADE OF CYLINDERS

A cascade of cylinders can show behavior similar to that of a cascade of airfoils. It can deflect a flow and produce an increase in static pressure. In addition, a cascade of cylinders has a characteristic frequency of vortex shedding. This information suggests the possibility of rotating stall (or phased vortex shedding) existing in a cascade of cylinders. To investigate this possibility, a set of cylinders of 0.50-inch diameter was made and installed in the circular-cascade test section with cascade solidities (cylinder diam./spacing) of 0.50 and 0.25. With a solidity of 0.50, a large pressure drop across the cascade was measured at all angles of attack. The flow was fully separated behind the cylinders at all inlet angles with large wakes of width approximately equal to the cylinder diameter. No phenomenon resembling rotating stall was observed, although at some inlet angles large velocity fluctuations of a random nature were found with a hot wire placed just upstream of the cascade. The diametral Reynolds number was 6×10^4. With a solidity of 0.25, a pressure rise was observed across the cascade at inlet angles greater than 60°, and C_p attained a peak value of 0.4 at 78°, decreasing rapidly at higher angles. Large random fluctuations in velocity ahead of the cascade were observed just after the peak on the C_p curve, but the schlieren photographs showed nothing which resembled rotating stall. Because of lack of time, the investigation was terminated at this point. Any further work on cascades of cylinders should probably be directed toward the low Reynolds number regime (less than 2×10^4) where vortex formation occurs close to the cylinder, and the vortices would have more influence on adjacent cylinders.

STOPPING THE ROTATING STALL PATTERN IN AN AXIAL COMPRESSOR

In an investigation of the flow in and around a stall cell, the major difficulty is measurement of velocities and directions in an unsteady flow. Hot wires are still not entirely satisfactory for measurements of unsteady velocities, especially where large angle fluctuations occur. If the stall pattern was stationary, conventional instruments could be employed to determine the limits of the stalled zone and the flow pattern in and around it. A study of the velocity triangles shows how this objective may be attained. With the stall cell propagating against the direction of rotation of the rotor with velocity V_p relative to the rotor, the absolute velocity of propagation is then $U - V_p$. In order to halt the stall cell, U must equal V_p. In the isolated rotor with 65-series blades, V_p was approximately $0.4\ W_{\theta,1}$. If it is assumed that this relation would be unchanged by preswirl when the guide vanes were a considerable distance upstream of the rotor, the stall cell would be stopped when $U = 0.4\ W_{\theta,1}$. The value $C_{\theta,1}$ must be approximately 1.5 U in the direction opposite to that of rotation because $W_{\theta,1} = U - C_{\theta,1}$.

Considerable counterswirl is therefore required, and for β_1 to be 75°, α_1 must be 66°. The work done by the rotor becomes a very small fraction of the kinetic energy leaving the guide vanes and entering the rotor so that it is impossible to stop the cell in a simple guide-vane and rotor combination. The losses in the system are so high that an additional booster fan is required. With a blower, which produced a boost pressure of 3 inches of water at the inlet of the axial compressor, calculations showed that it would be possible to halt the stall cell with values of β_1 equal to or higher than 75° at a compressor speed of 1000 rpm. Lower values of β_1 could not be attained at this compressor speed because of the high losses in the system. A set of adjustable preswirl vanes was constructed and installed in the radial inlet of the single-stage compressor (fig. 14), and a blower with a capacity of 16,000 cubic feet per minute at a delivery pressure of 3 inches of water was mounted beside the compressor, feeding air to the compressor intake through a balloon-type plenum chamber made of thin plastic sheet. The complete arrangement is shown in figure 15, with the compressors running and the plenum inflated. A large number of static-pressure taps were drilled in the casing around the circumference ahead of and behind the rotor, and the leads were connected to a bank of manometer tubes. In addition, instrumentation for determining flow angle and stagnation pressure was installed upstream of the rotor, and two Kiel probes were installed downstream.

The manometer board arrangement is shown in figure 16. The zero reading is given by the left-hand tube on both boards. The next three tubes on the left-hand board show upstream and downstream stagnation pressures, and the remainder give static-pressure readings.

With some trial-and-error adjustment of the compressor speed and guide vanes, it was found possible to stop the stall pattern over a range of β_1 close to the predicted values. The best indication of a stationary cell was the bank of manometer tubes, which clearly showed the moving pressure wave when the absolute rotational speed fell below 1 rps. With proper adjustment the pressure wave could be held stationary for several seconds, and photographs of the pressure distribution could be taken before some disturbance caused movement of the pattern. A typical standing wave is shown in figure 17. At this point, β_1 was 74° at the mean radius, and α_1 was 59°. Previous tests on the isolated rotor suggested that two or more cells should have been present at this point, but only one cell was found, and $V_p/W_{\theta,1}$ was 0.5 instead of 0.4. The change in the stall-cell pattern may have been due to the nonuniform character of the flow entering the rotor, since the preswirl vanes set up a free vortex-swirl distribution, with a resulting angle distribution quite unlike that for which the rotor was designed. The stall cell extended from root to tip of the blades.

With a further increase in α_1, the stall cell could be made to rotate slowly in the direction opposite to that of the rotor. In reference 4, experiments with adjustable guide vanes are described in which no change in the absolute stall-propagation speed was found when the guide-vane angle was changed. When the results reported herein are considered, it appears that guide-vane interference was responsible for the invariance of V_p in the NACA tests.

With the stall cell stationary, a remarkable confirmation of the hypothesis of zero velocity in the cell could be obtained simply by examining the exhaust leaving the rear of the compressor. Over a substantial portion of the annulus no flow could be detected. Analysis of the pressure patterns from the manometer boards also confirmed several other ideas (fig. 17). In part of the stall cell, there was no pressure change across the blade row. Over the remainder of the cell there appeared to be some pressure rise, but the upstream pressure measurements were made 2 chord lengths from the blade row. Measurements made closer to the blade row would probably show higher upstream pressures. The circumferential pressure variation downstream of the blade row was much smaller than that upstream, and the mean downstream pressure was equal to the upstream pressure plus 0.85 of the dynamic pressure relative to the stall cell (apparently substantiating the simple analysis of the section EQUILIBRIUM OF STALL CELL AT CASCADE).

The useful results obtainable from the modification of an air compressor are limited, but, if the basic ideal of stopping the cell pattern is proved practicable, it appears that experiments on a machine with a transparent casing would yield information on the general phenomenon and might provide a basis for a method of predicting the number of cells. A water-pump rig might be particularly suitable for this work. Another interesting field for investigation is the effect of radial equilibrium and rotation on stall propagation. This could be studied by varying the guide-vane angle while adjusting the pump speed to keep β_1 constant. Any variation in stalled behavior would then be due to the variation in centrifugal field. The substantial swirl change from root to tip in the Gas Turbine Laboratory rig prevented an investigation of this type because β_1 could be maintained constant only at the mean radius, large changes occurring elsewhere when the guide-vane angle and compressor speed were altered.

CONCLUSIONS

The small perturbation analyses of rotating stall appear to give a good understanding of the stability conditions which govern the initiation of rotating stall, while the fully developed phenomenon can be represented by the model developed by Kriebel, Seidel, and Schwind. However, no one theory predicts the propagation speed accurately for all the experimental configurations tested, and the factors governing the number of stall cells remain undetermined. The major unknown is the response of the

boundary layer to an unsteady flow field, and it is suspected that little progress will be made on the rotating-stall problem until the boundary-layer behavior is understood.

The demonstrated ability to stop the rotating-stall pattern in a compressor stage should facilitate a closer examination of the stall cell and the splitting process if suitable flow visualization techniques can be developed. A water pump may be suitable for this purpose.

Massachusetts Institute of Technology,
Cambridge, Mass., August 12, 1957.

REFERENCES

1. Stenning, Alan H., Kriebel, Anthony R., and Montgomery, Stephen R.: Stall Propagation in Axial Compressors. NACA TN 3580, 1956.

2. Montgomery, S. R., and Braun, J. J.: Investigation of Rotating Stall in a Single-Stage Compressor. NACA TN 3823, 1957.

3. Emmons, H. W., Pearson, C. E., and Grant, H. P.: Compressor Surge and Stall Propagation. Trans. ASME, vol. 77, no. 4, May 1955, pp. 455-467; discussion, pp. 467-469.

4. Costilow, Eleanor L., and Huppert, Merle C.: Some Effects of Guide-Vane Turning and Stators on the Rotating Stall Characteristics of a High Hub-Tip Ratio Single-Stage Compressor. NACA TN 3711, 1956.

5. Kriebel, Anthony R., Seidel, Barry S., and Schwind, Richard G.: Stall Propagation in a Cascade of Airfoils. NACA TN 4134, 1958.

6. Lamb, Horace: Hydrodynamics. Dover Pub., 1945, pp. 101-103.

7. Wood, M. D.: Stall Propagation in Axial Flow Compressors. Ph.D. Thesis, Cambridge Univ., May 1955.

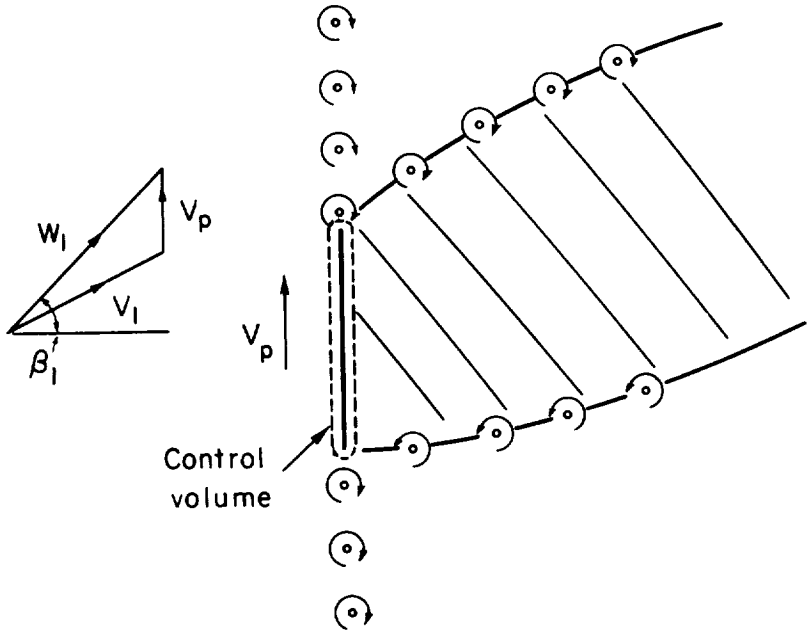

Figure 1. - Model of stall propagation.

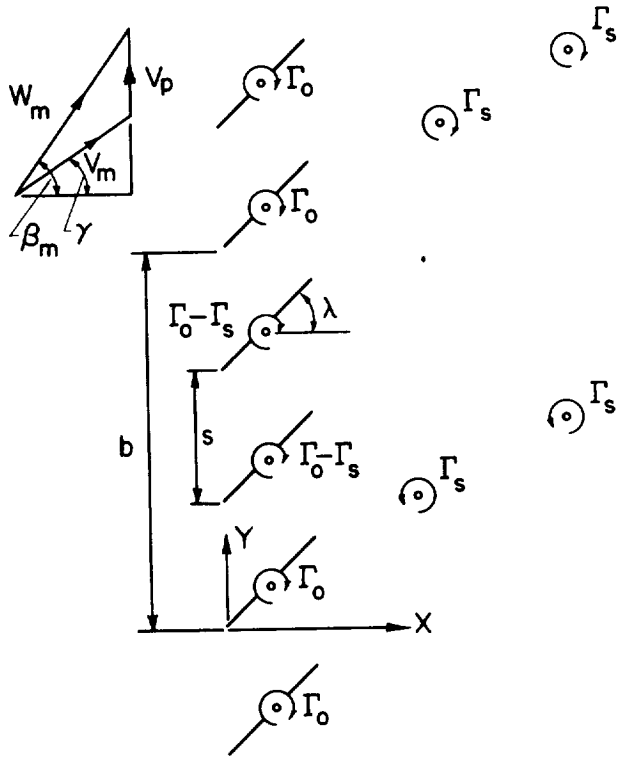

Figure 2. - Representation used for numerical analysis.

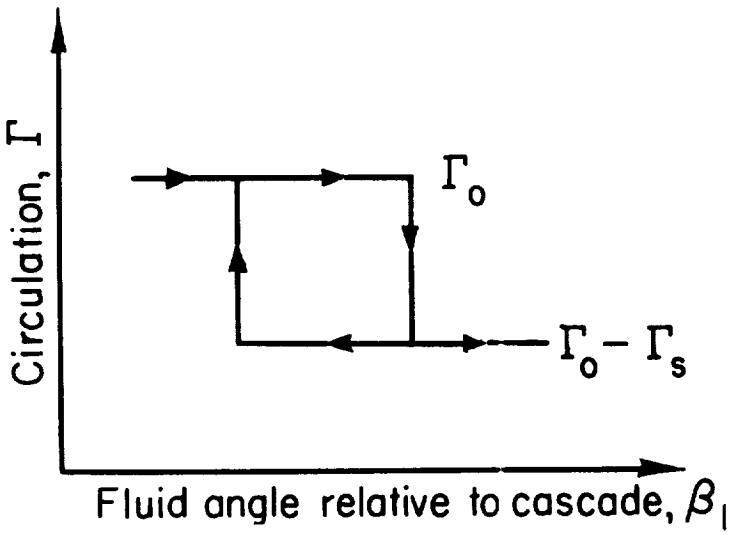

Figure 3. - Cascade characteristic.

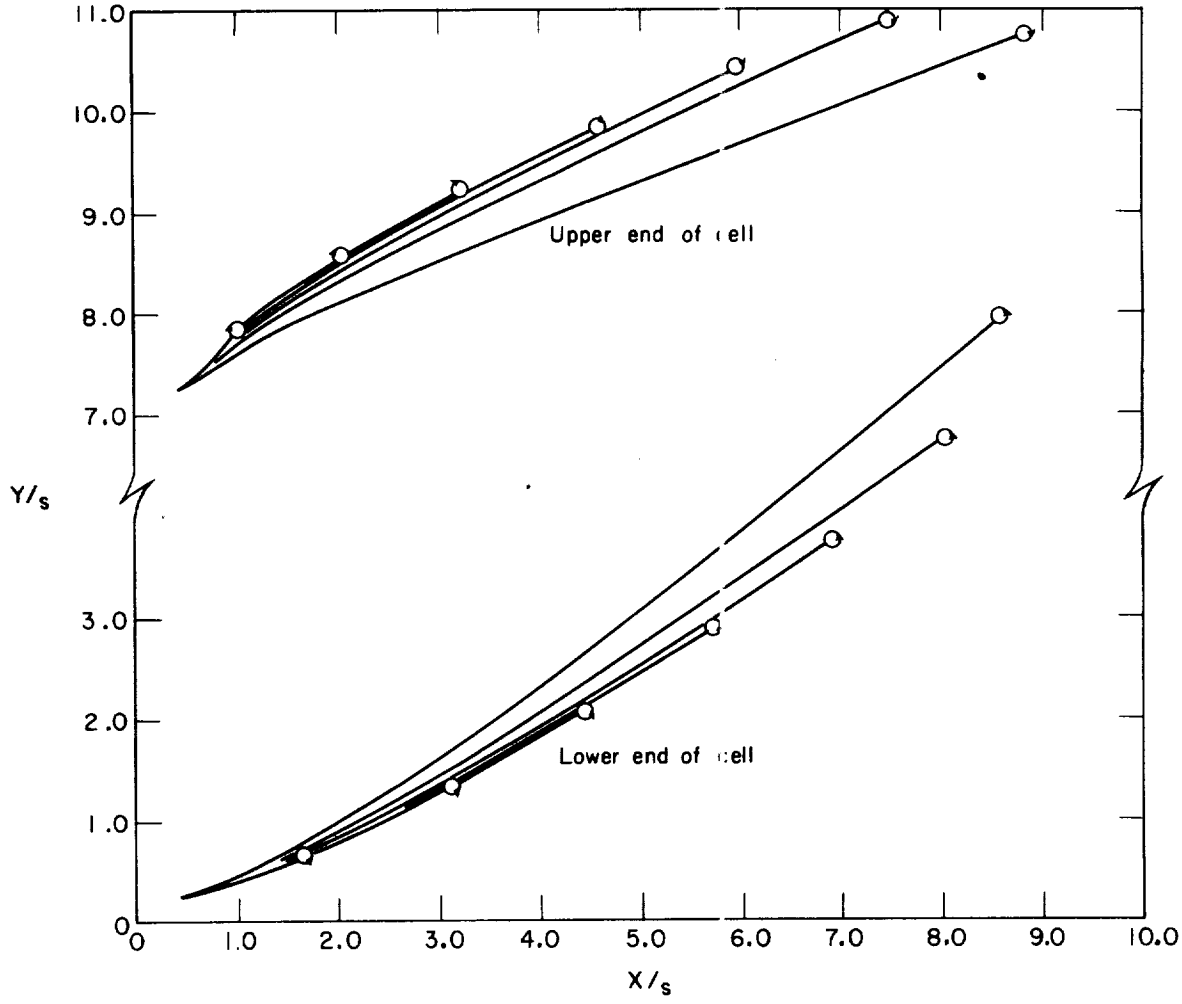

Figure 4. - Vortex trajectories.

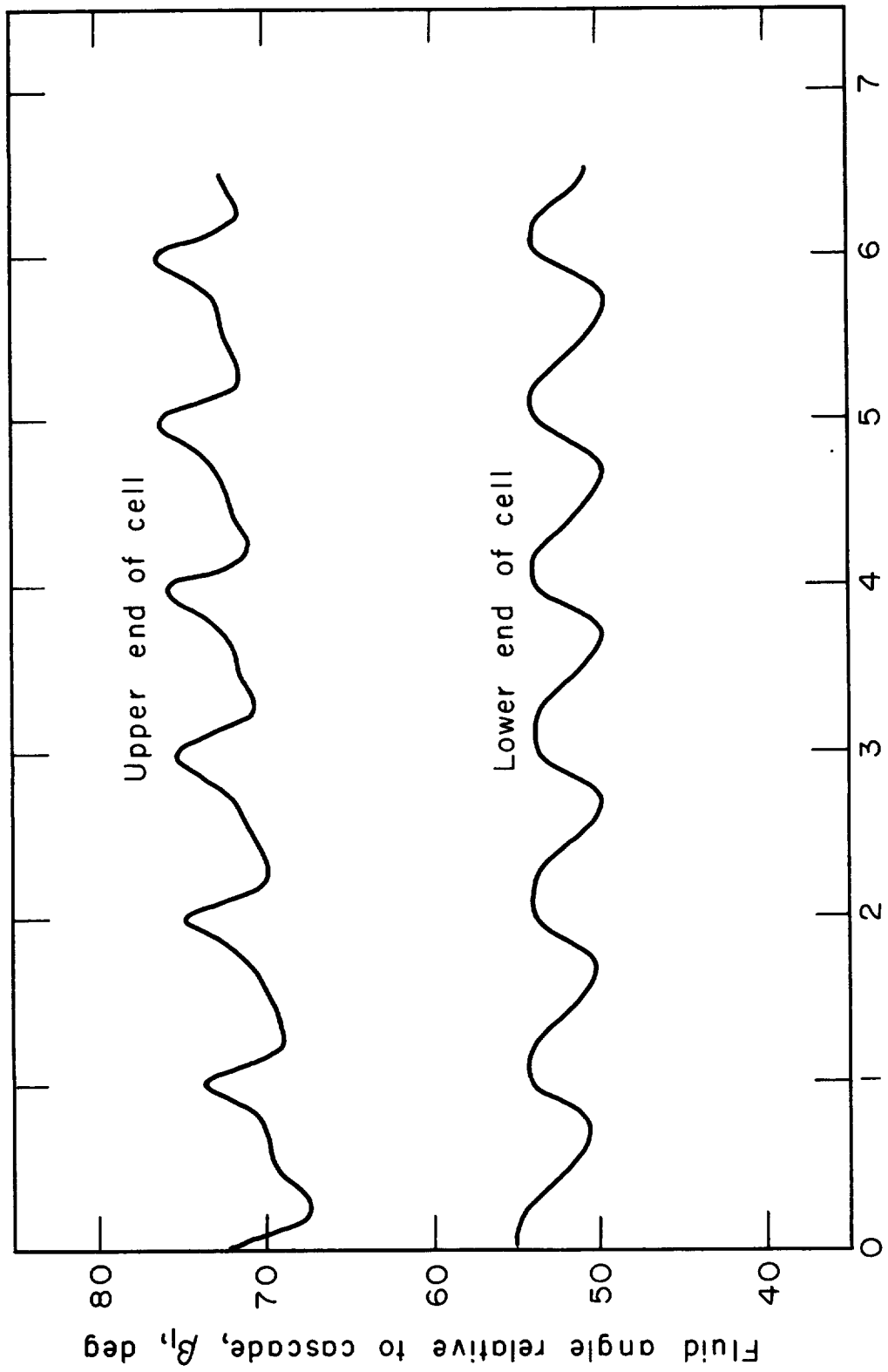

Figure 5. - Flow angles at ends of stall cell.

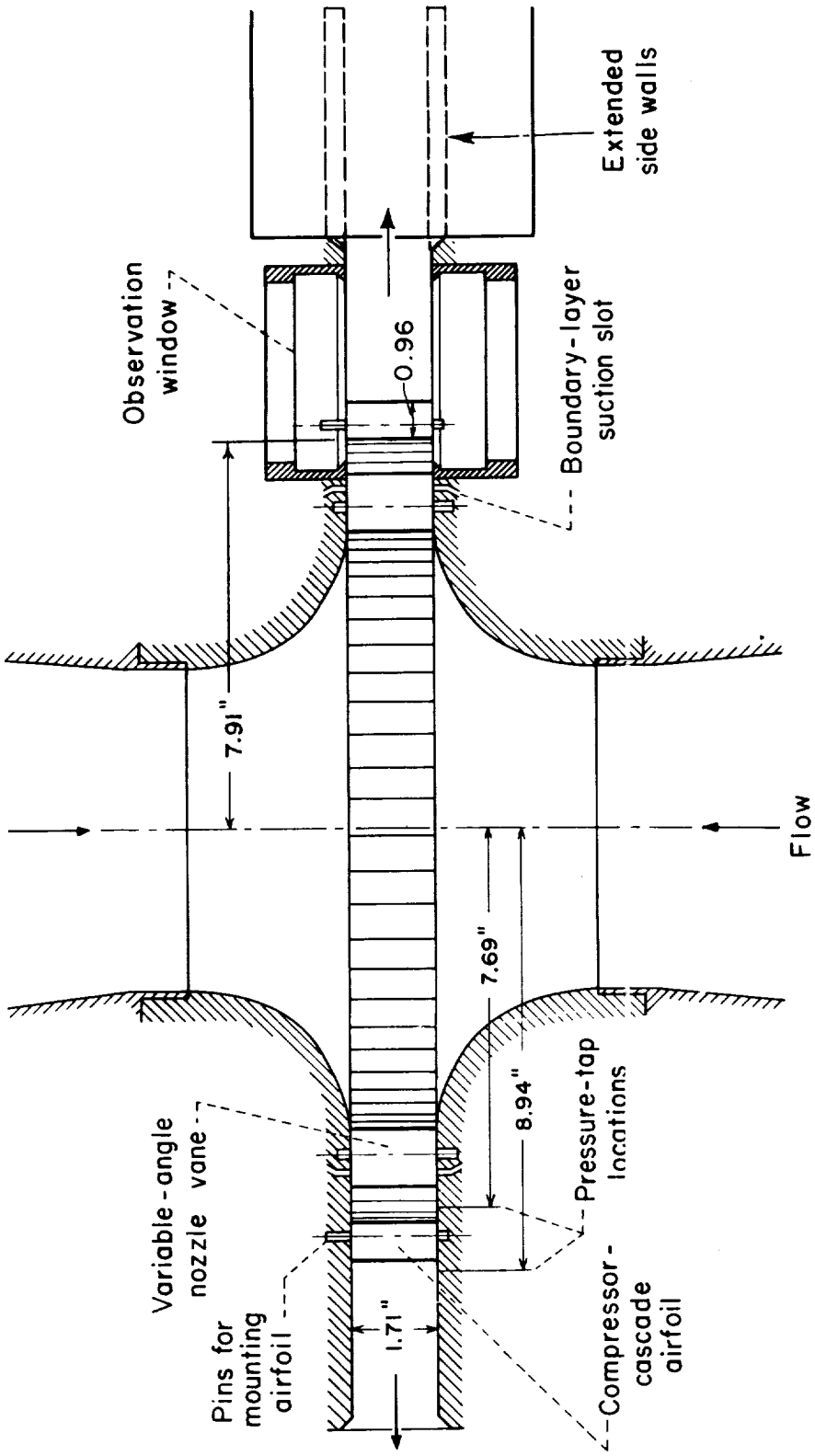

Figure 6. - Schematic diagram of circular cascade test section.

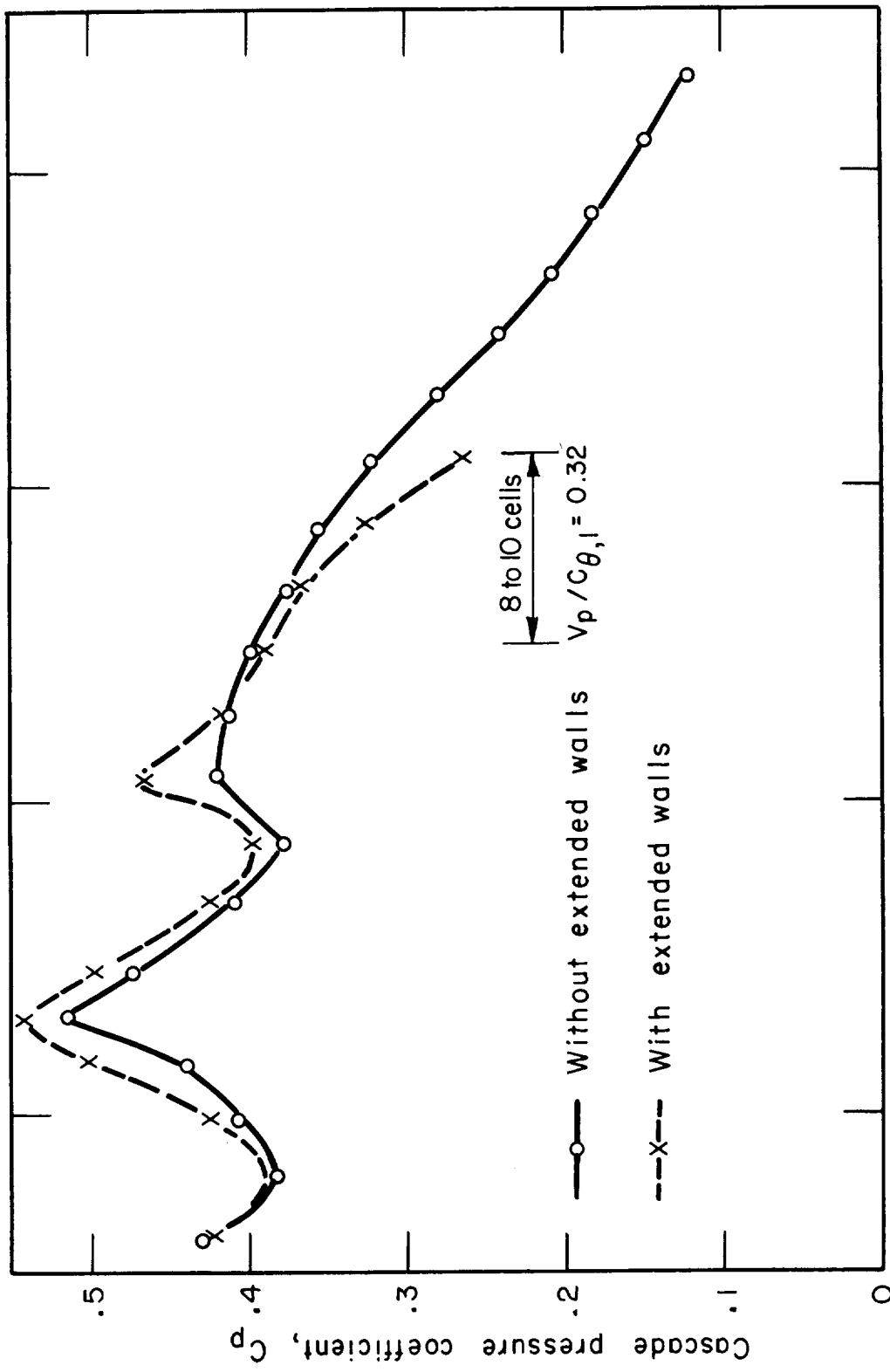

Figure 7. - Performance of high-camber blading at stagger angle of 31°.

Without extended side walls

← Time

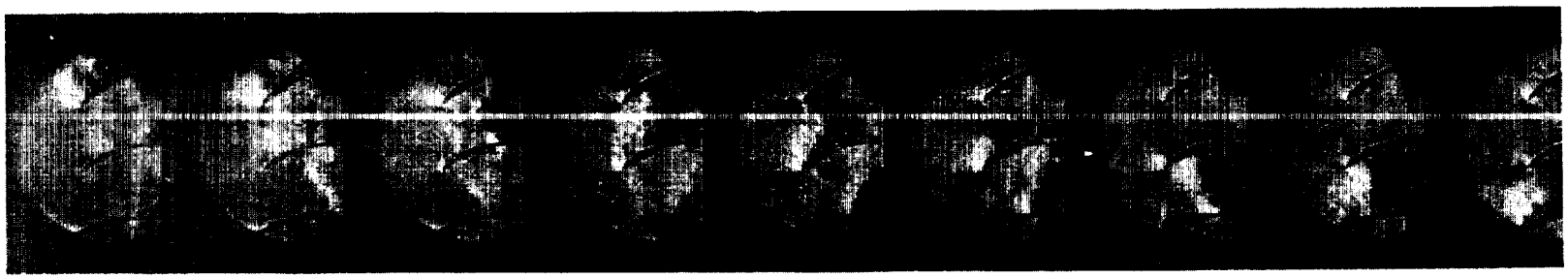

With extended side walls

(a) Mach number, 0.36; fluid angle relative to cascade, 65°.

Figure 8. - Schlieren photographs of high camber blading at stagger angle of 31°. Frames per second, 5,000.

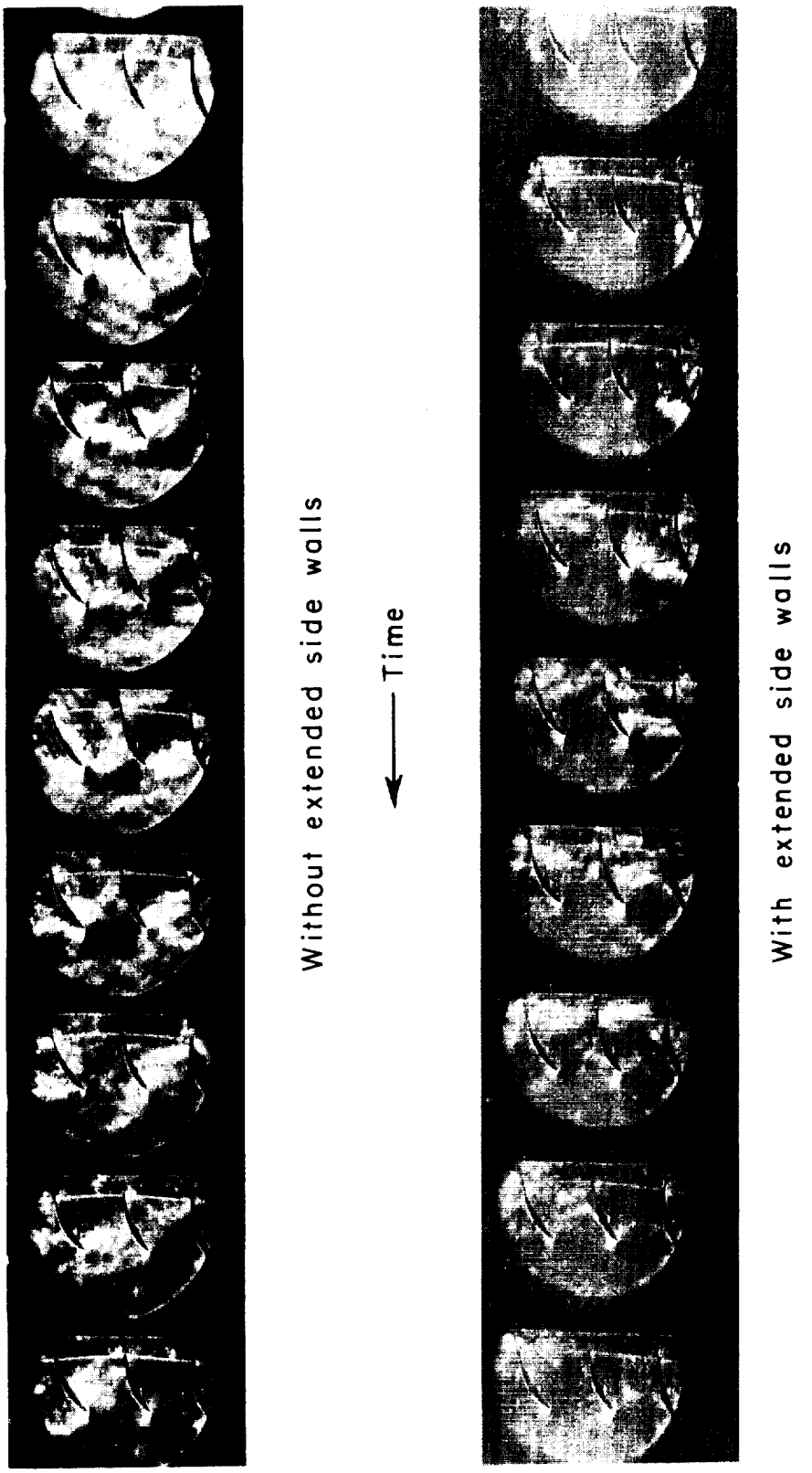

(b) Mach number, 0.35; fluid angle relative to cascade, 71°.

Figure 8. - Continued.

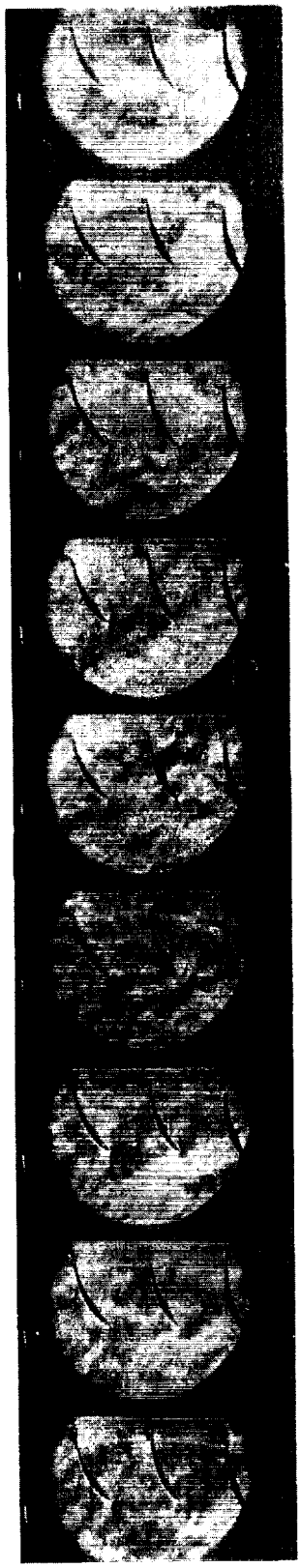

(c) Mach number, 0.47; fluid angle relative to cascade, 33°.

Figure 8. - Concluded.

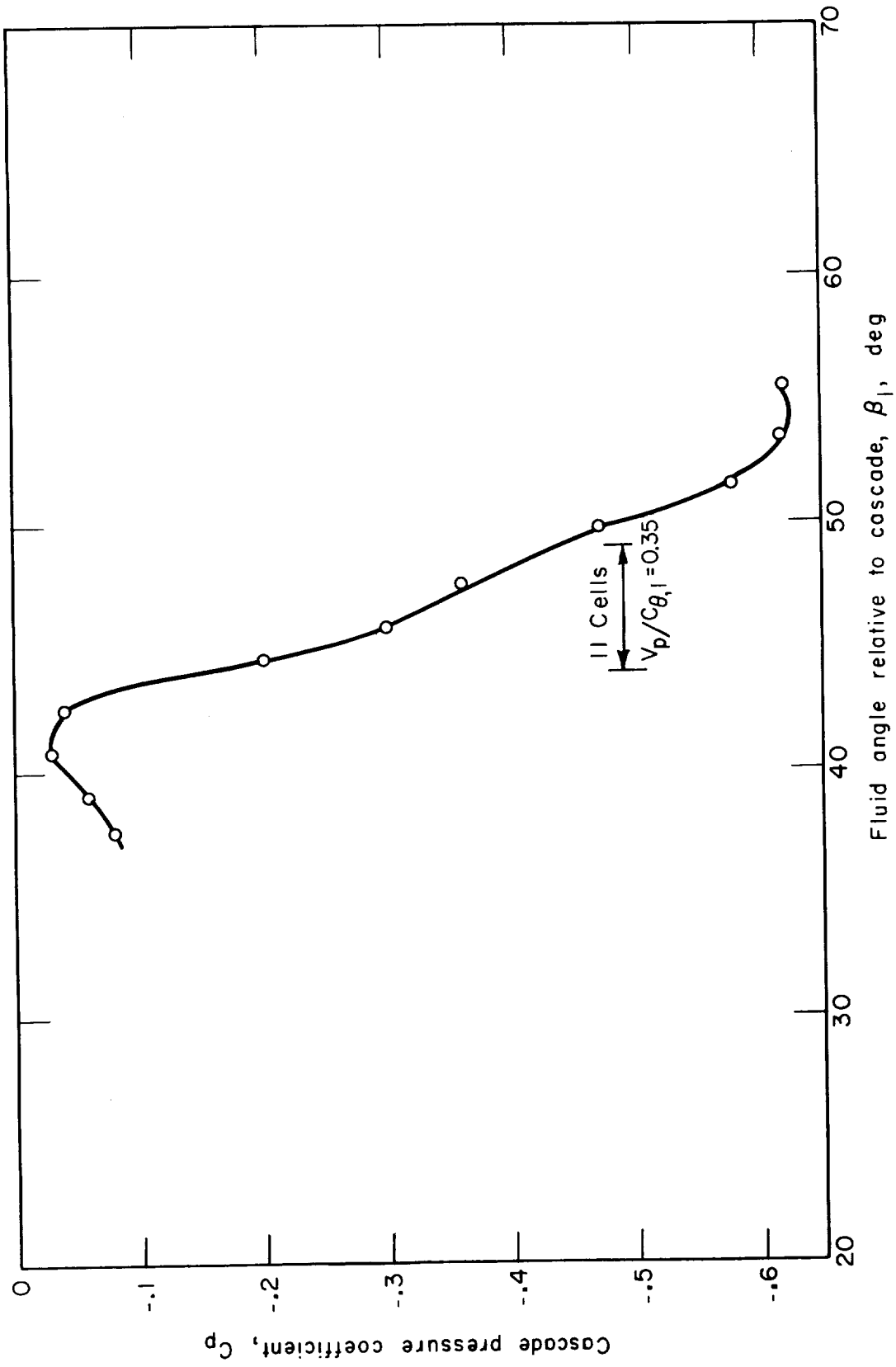

Figure 9. - Cascade pressure coefficient against fluid angle relative to cascade for high-camber blading. Blade stagger angle, 0°.

Figure 10. - Schlieren photographs of high camber blading at blade stagger angle of zero; Mach number, 0.22; fluid angle relative to cascade, 44°, frames per second, 5,000.

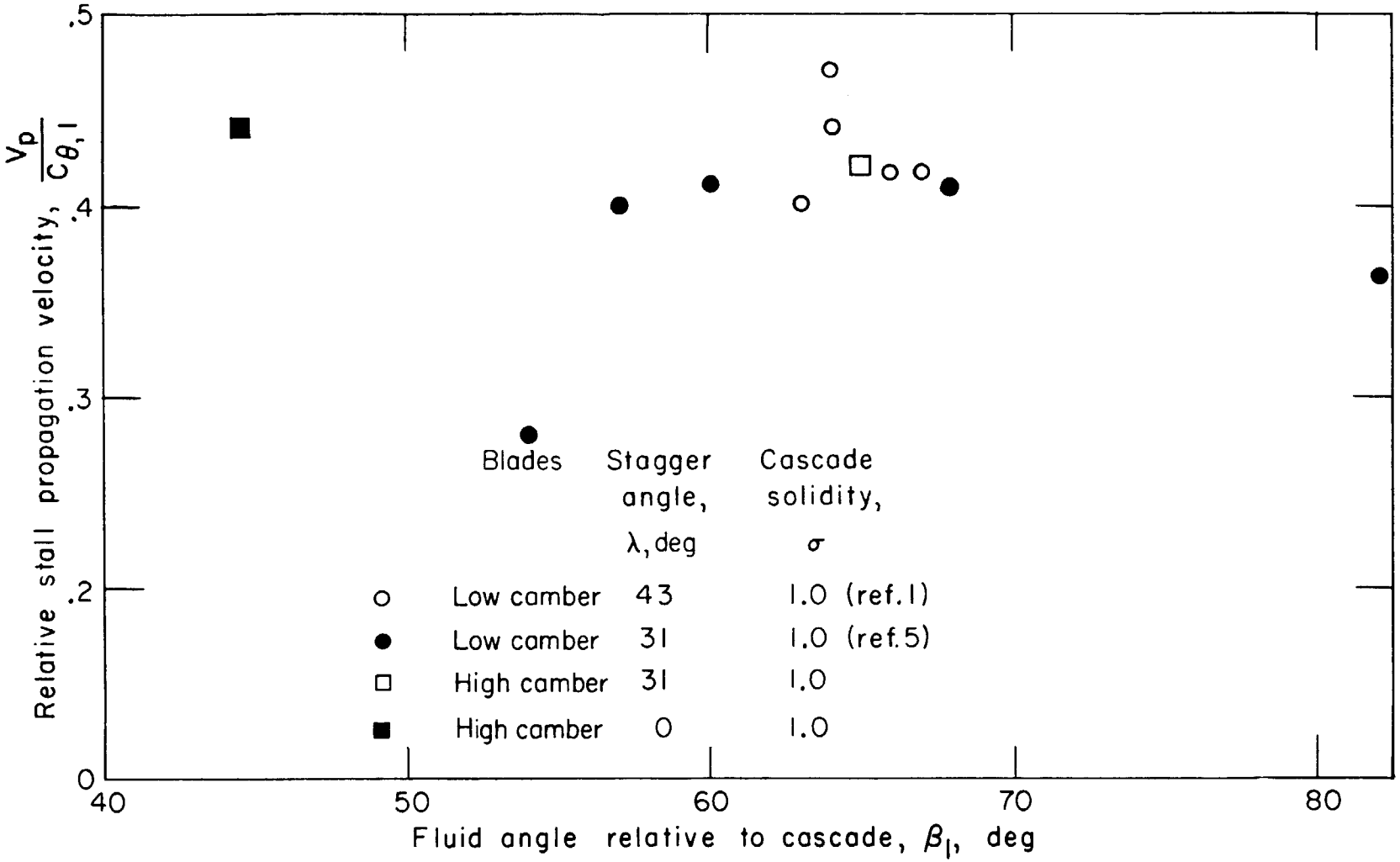

Figure 11. - Propagation velocities in the circular cascade; cascade solidity, 1.0.

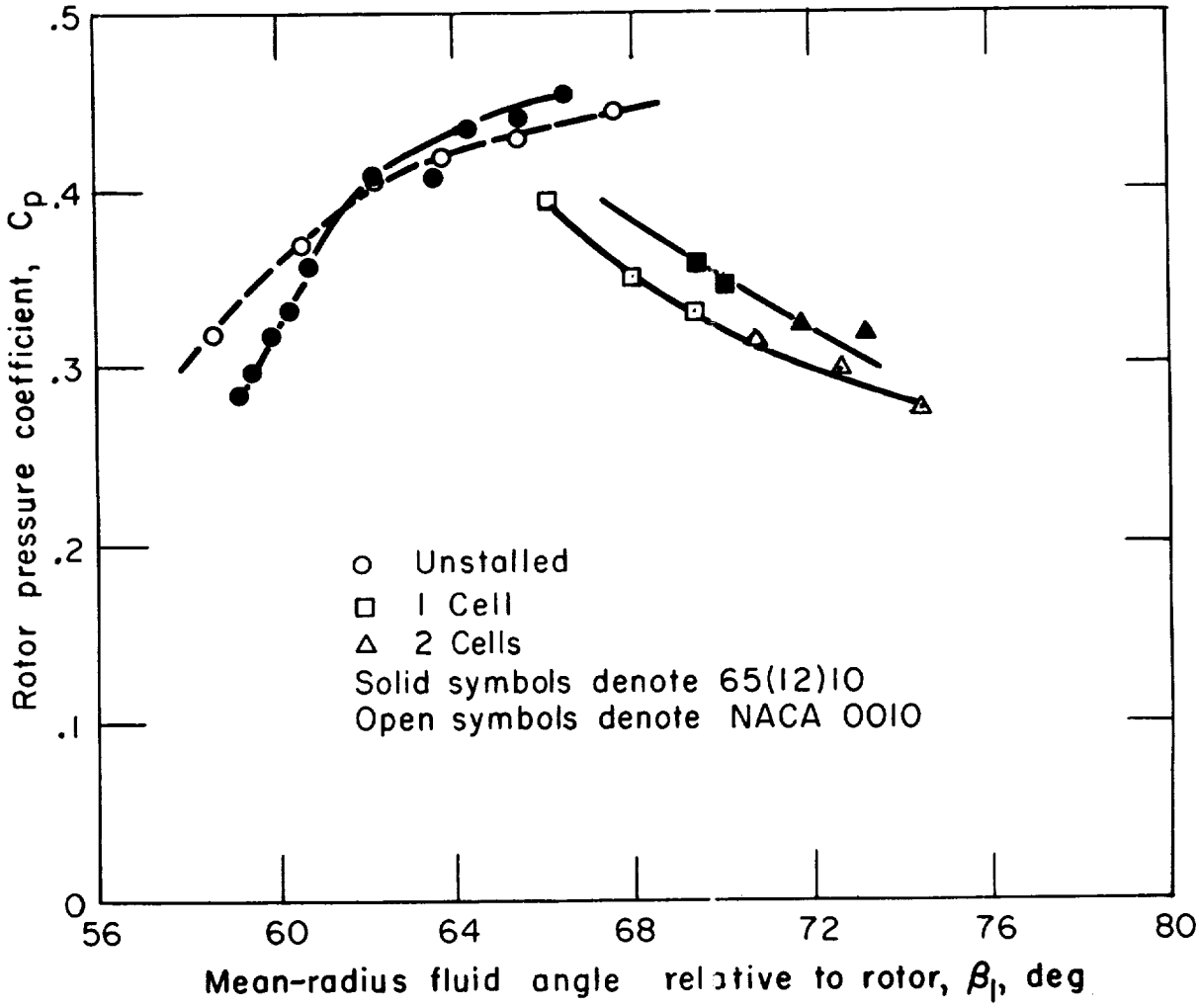

Figure 12. - Performance of isolated rotor.

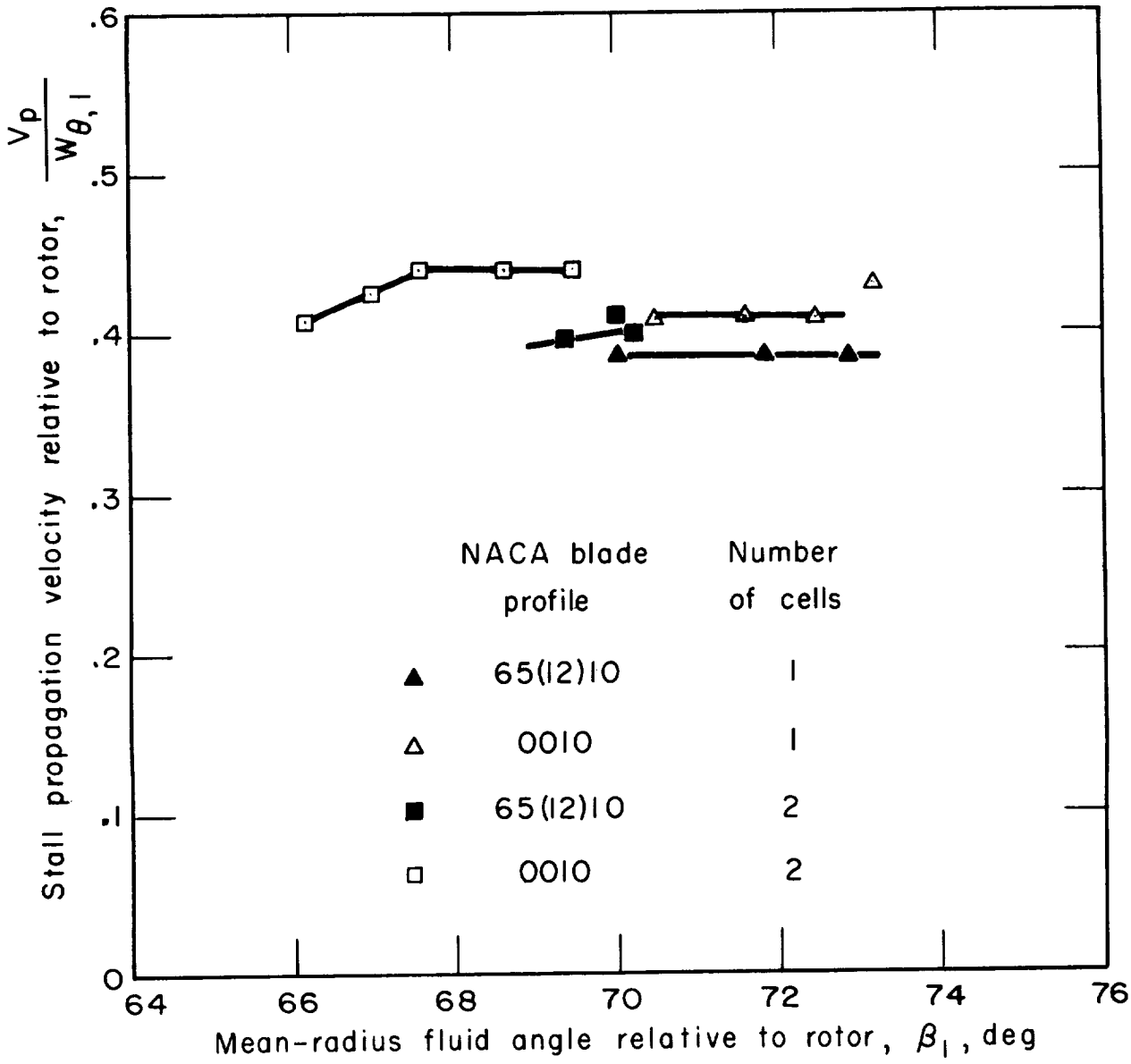

Figure 13. - Propagation velocities in the rotor.

Figure 14. - Preswirl vane arrangement in the axial compressor.

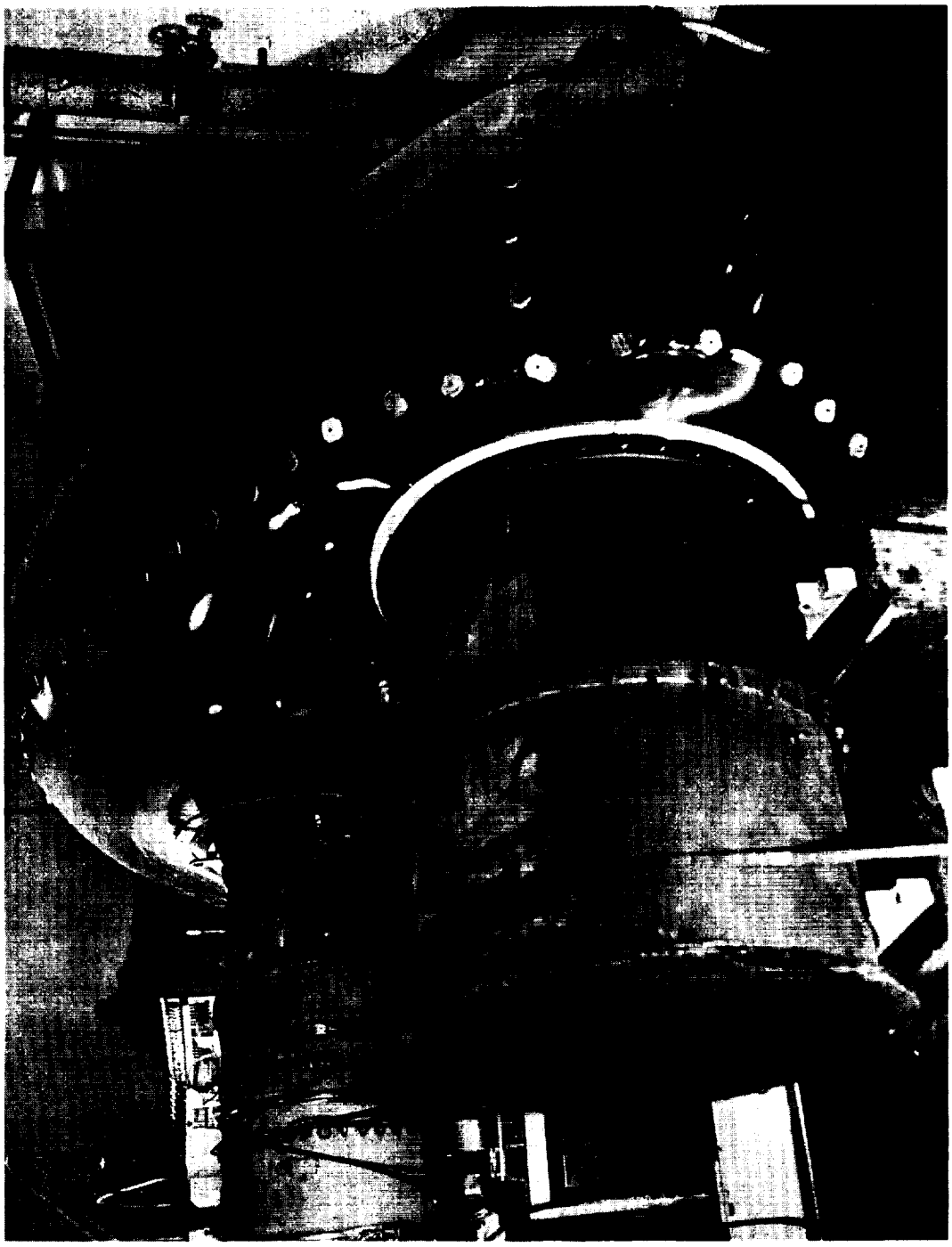

Figure 15. - Single-stage compressor with booster fan and plenum.

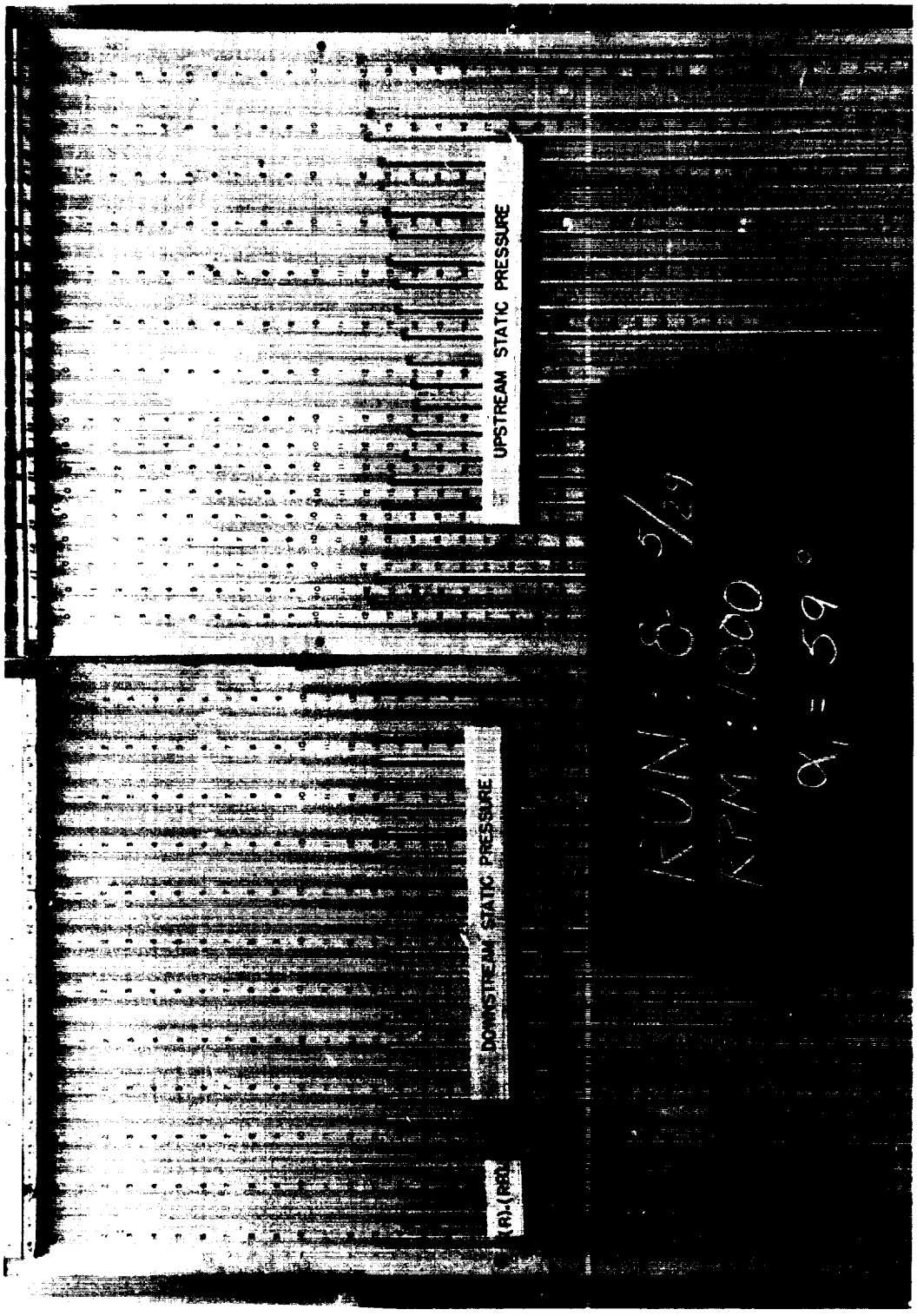

Figure 16. - Pressure pattern with stationary stall cell; mean-radius fluid angle relative to rotor, 74°; absolute fluid angle, 59°.

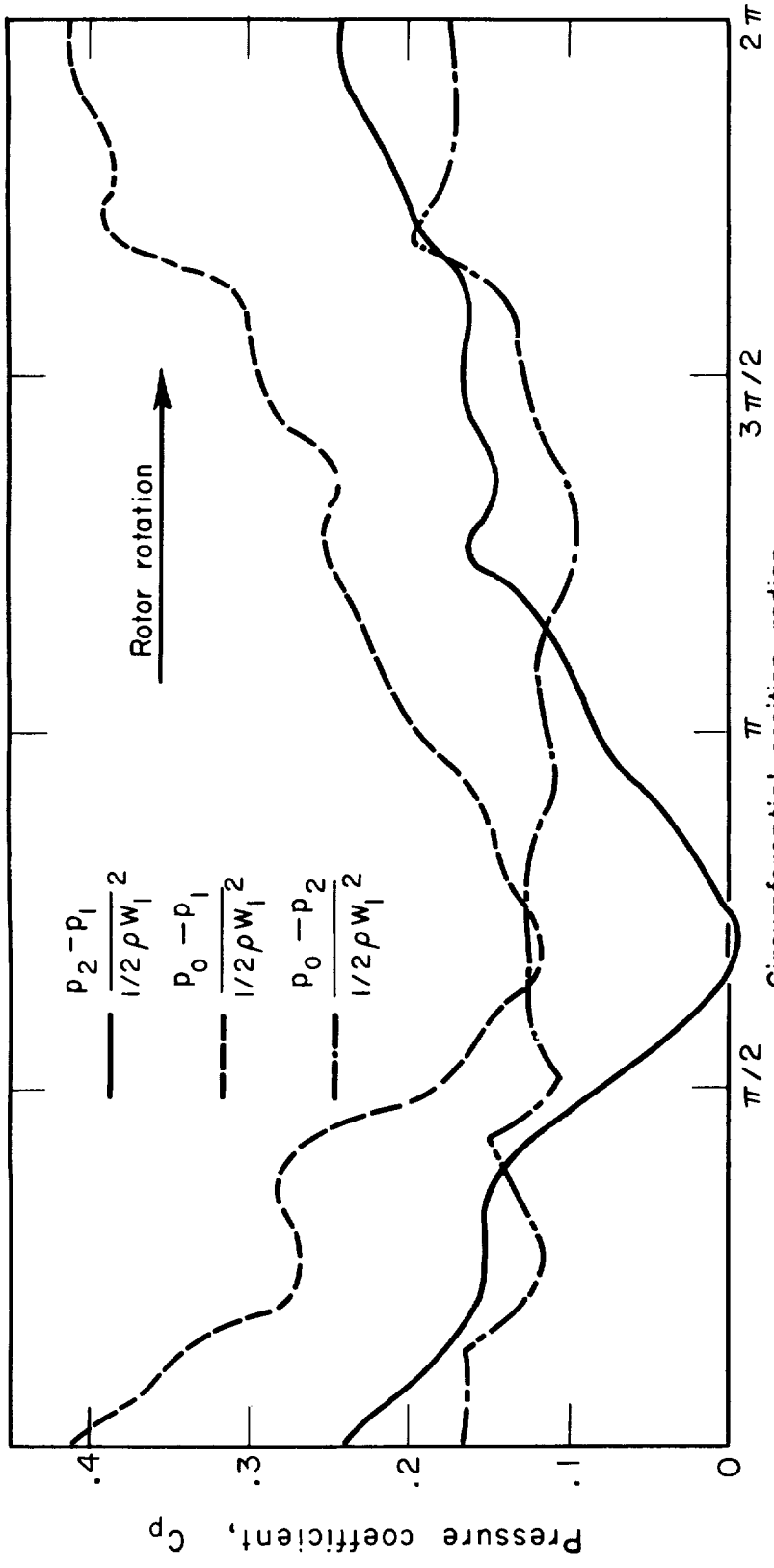

Figure 17. - Circumferential pressure variation; mean-radius fluid angle relative to rotor, 74°; absolute fluid angle, 59°.

NASA - Langley Field, Va. 5081